

Quantitative Scanning Probe Microscopy for Nanomechanical Forensics

F.W. DelRio¹ · R.F. Cook²

Received: 13 June 2016 / Accepted: 20 October 2016 / Published online: 31 October 2016
© Society for Experimental Mechanics (outside the USA) 2016

Abstract Atomic force microscopy (AFM) was used to assess the indentation modulus M_s and pull-off force F_{po} in four case studies of distinct evidence types, namely hair, questioned documents, fingerprints, and explosive particle-surface interactions. In the hair study, M_s decreased and F_{po} increased after adding conditioner and bleach to the hair. For the questioned documents, M_s and F_{po} of two inks were markedly different; ballpoint pen ink exhibited smaller variations relative to the mean value than printer ink. The fingerprint case study revealed that both maximum height and F_{po} decreased over a three-day period. Finally, the study on explosive particle-surface interactions illustrated that two fabrics exhibited similar M_s , but different F_{po} . Overall, it was found that AFM addresses needs in forensic science as defined by several federal agencies, in particular an improved ability to expand the information extracted from evidence and to quantify its evidentiary value.

Keywords Forensic science · Scanning probe microscopy · Mechanical properties · Trace evidence · Questioned documents · Fingerprint residue · Explosive materials

✉ F. W. DelRio
frank.delrio@nist.gov

R. F. Cook
robert.cook@nist.gov

¹ Applied Chemicals and Materials Division, Material Measurement Laboratory, National Institute of Standards and Technology, Boulder, CO 80305, USA

² Materials Measurement Science Division, Material Measurement Laboratory, National Institute of Standards and Technology, Gaithersburg, MD 20899, USA

Introduction

Many forensic analysis techniques generate information about how objects “look” to provide guidance for police investigations or evidence for use in legal cases. Examples include the particular features appearing in a fingerprint, the color of a paint chip, the striation pattern on a fired bullet, the line crossings in a written text, and the swelling or shrinkage of an environmentally-exposed fiber. Together with chemical analyses, such information enables the material forming an object and the object history to be identified. However, forensic analyses could generate significantly more information and thus better evidence if, in addition to providing information about how an object looks, analyses could provide information on how an object “feels.” This is because how an object feels—its mechanical response—is also deeply dependent on the material forming the object and the object history. For example, the stiffness of natural and synthetic fibers differs greatly, and exposure to water alters the stiffness of each in different ways. Hence, development of quantitative methods to measure the mechanical responses of objects used in investigations and evidence would be a significant advance in forensic analyses. Scanning probe microscopy techniques—in particular atomic force microscopy (AFM)—provide a means for imaging objects *and* measuring mechanical properties at different length scales.

This paper makes the case that AFM has great potential as a technique in forensic evidence applications. The case is made by demonstrating in a series of examples how AFM measurements can be quantified, extending the technique beyond qualitative comparison of raw data. Specifically, the examples illustrate how a simple analysis method can be used to quantify two common features of material mechanical response: the elastic modulus and the pull-off force, the latter of which is related to the work of adhesion. It is recognized that this is

only the first step in establishing AFM as a quantitative forensic evidence tool. The necessary second, and larger, step is quantification of the reproducibility of AFM measurements so as to provide a measure of the probability that an AFM-measured quantity represents a particular material. Such quantification requires detailed statistical studies and must thus be the subject of future, larger, works focused on specific forms of evidence. In order to provide context for the examples to follow, the previous use of AFM in forensic applications is briefly reviewed, and the level of quantitative analysis assessed.

There have been several illustrations of AFM *imaging* for forensic applications: Quantitative analysis of human hair cuticles verified the usefulness of high-resolution AFM images in classifying hair samples [1–8]. AFM images of ink line crossings have been exploited to provide qualitatively similar information to that obtained with scanning electron microscopy (SEM) [8, 9]. AFM imaging of gunshot residue was used to illustrate the morphology and distribution of residue particles and to deduce shooting distance [10, 11]. AFM images of materials exposed to ionizing radiation identified characteristic radiation defects that could be used in dosimetry [12]. Time-lapsed AFM images of blood cells revealed changes in cell morphology with time and the possibility of using observations of these changes to estimate time of death [13–15]. AFM images have revealed sizeable variations in the morphology of various viruses and bacterial spores, and how these variations change with the nutrient exposure [16]. AFM images have been used to image fingerprint residue [17] and powder spray [8] and to set the baseline structures of polymeric [18] and metallic [19] surfaces employed in latent fingerprint development. Statistical analyses of AFM topography measurements of textile fibers exposed to environmental stress were used to illustrate the ability of nanoscale images to distinguish different environmental exposures [20]. AFM images have also been used to distinguish various adhesive tapes [21]. Finally, AFM images of different explosive particles and substrates have been used to analyze the morphology of the particles and substrates [22, 23].

There have been fewer examples of AFM *mechanical properties measurements* for forensic applications: Characterization of the mechanical properties of human hair cuticles was performed as a function of treatment type [3, 4, 6, 24], ethnicity [6], and environment [7]. Differences in the mechanical responses of fingerprint material and a glass substrate were demonstrated in air and water, although the data were not analyzed to extract mechanical properties [17]. Changes in the stiffness of blood spots with drying time on glass were demonstrated and the data were analyzed assuming an ideal elastic response to show an apparent increase in elastic modulus of the blood with time [14]. However, data were not provided to support the elastic assumption and the effects of the glass substrate were not taken into account. The effects

of drying time on individual red blood cells on glass and mica substrates were quantified in terms of the adhesion force between a sharp silicon probe and the cells, after exposure to indoor and outdoor conditions [15]. AFM force-displacement curves were examined on a series of adhesive tapes and interpreted in terms of the force and displacement required to break the probe-tape bond [21]. Finally, AFM force spectroscopy was used to consider the adhesive forces between trinitrotoluene (TNT), cyclotrimethylenetrinitramine (RDX), and pentaerythritol tetranitrate (PETN) explosive particles and metallic and polymeric surfaces [22, 23, 25].

There are three striking features in considering the works cited above: The first is how few of them there are, just over two dozen, given that there are about 10,000 AFMs in use worldwide. Second, almost none of the works had any specific follow up research given the demonstrated potential for AFM use in forensics. A third feature perhaps explains the first two: Most of the works reported results simply as observations with no analysis or with only semi-qualitative analyses; current methods of calibration and analysis of AFM mechanical measurements were mostly not used. Without rigorous, accepted methods of quantitative analysis, in either the “measurement” or “probability” sense, the ability of AFM to generate supportable forensic evidence is limited. As a result, the driving force for follow up research and publications on applications of AFM in forensic analyses also remains limited. In this paper, we start to overcome this weakness by demonstrating broadly applicable, quantitative, traceable methods for applications of AFM in forensics on four types of evidence: trace evidence, questioned documents, impression and pattern evidence, and explosive materials. In particular, AFM is utilized to study the mechanical properties of hair as a function of treatment type, questioned documents as a function of ink type, fingerprint residue as a function of time, and explosive particle-surface interactions as a function of fabric type.

Materials and Methods

Methods

A schematic diagram of an AFM is shown in Fig. 1(a). Both measurement of mechanical properties and imaging of a sample are performed through interactions with a probe; the probe is attached to the end of a flexible cantilever that is attached to a holder controlled by the microscope. As the probe is moved over the sample by either sample stage or cantilever holder motion, mechanical interactions between the probe and the sample surface cause the cantilever to deflect. The deflection causes a laser beam that is reflected off the back of the cantilever to move over the surface of a photodiode detection system. In imaging mode, the probe is scanned parallel to the sample surface (with the xy scanner) and a feedback system coupled to the photodiode

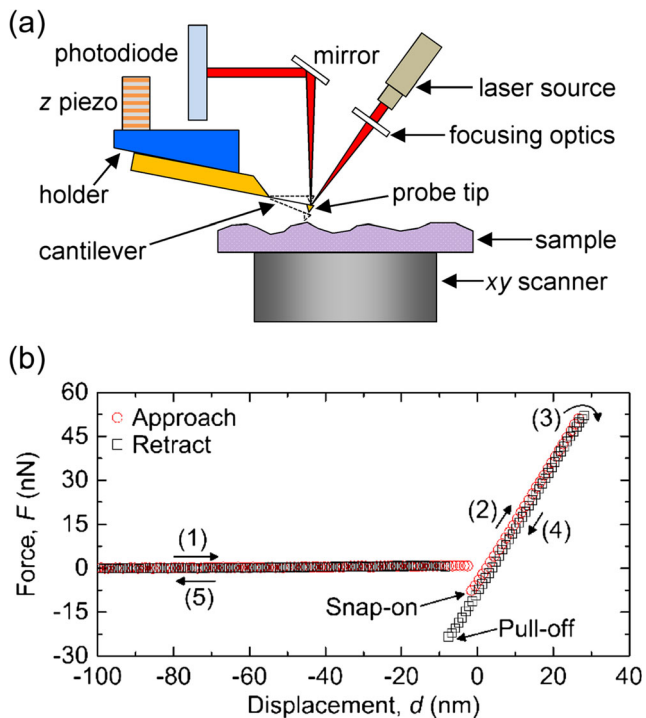


Fig. 1 (a) AFM schematic diagram. In mechanical measurement mode, the probe holder is moved perpendicular to the sample surface, and the deflection of the cantilever is measured as a function of the holder position. Appropriate calibration of the system allows the force exerted by the sample on the probe to be determined as a function of probe displacement relative to the sample surface. (b) AFM force-displacement data includes both the extension of the cantilever towards the sample surface (1, 2) to a peak load (3) and the retraction of the cantilever away from the sample surface (4, 5)

maintains the cantilever deflection at a desired set point via the action of a piezoelectric actuator (the *z* piezo); the feedback signal is used to generate a topographic image of the surface. However, the real forensic power of AFM lies in its ability to make localized mechanical properties measurements with great sensitivity. In mechanical measurement mode, the feedback system is turned off, the cantilever holder is moved perpendicular to the sample surface, and the deflection of the cantilever is measured as a function of the holder position. Appropriate calibration of the system enables the force *F* exerted by the sample on the probe to be determined as a function of the holder displacement *d*, an example of which is shown in Fig. 1(b). The *F*-*d* data include both the extension (loading) of the cantilever towards the sample surface to a peak load and the retraction (unloading) of the cantilever away from the surface. Appropriate analysis of the *F*-*d* data enables mechanical properties of the sample to be determined; the probe can be moved to various locations on the sample to form maps of mechanical properties as shown later. As measurements of cantilever deflection determine *F*, cantilever compliance is selected so as to provide maximum sensitivity within the limits of the photodiode range, but not so great that the “snap-on” and “pull-off” instabilities [26] visible in Fig. 1 dominate the *F*-*d* behavior.

AFM measurements can be customized in many ways: Different tips can be used to probe different aspects of mechanical properties. For example, a conventional “sharp” silicon or silicon nitride tip is used for imaging and local property measurements with nanometer lateral resolution. A spherical probe tip, or “colloidal” probe, is used to generate spatially-averaged measurements with micrometer resolution. An advantage of colloidal probe measurements is that the probe material and size can be customized to investigate a specific material-material mechanical interaction. For example, the adhesion between an explosive particle (the probe) and a fabric (the sample) could be measured. The forces used in AFM measurements are small, from nanonewtons to micronewtons (one nanonewton is about the weight of a pollen grain), and hence AFM measurements are minimally invasive. In many cases, the probe interacts with the sample via short range surface forces or liquid capillary menisci. When the probe is in contact with the sample, lateral motion imposed on the probe causes the cantilever to twist and, after appropriate calibration, the lateral force between the probe and the sample can also be measured. Finally, AFM measurements can be performed in environments from ultra-high vacuum to liquids such as water and require very small amounts of sample material.

The basic experimental method here was similar for all four evidence types; the mechanical properties were measured with a commercially-available AFM at 25 °C in ambient conditions using an AFM probe with a spring constant *k_c* as measured by the thermal fluctuation method [27]. Each sharp or colloidal probe was inspected before and after force measurements via SEM to assess the tip radius *R* and check for damage or material transfer; *R* was found to be ≈ 40 nm for the sharp silicon probes and ≈ 12 μm for the colloidal probes, and no damage or transfer was observed. In order to determine mechanical properties, the deformation of the sample surface δ by the probe is required. Hence, force-deformation (*F*- δ) data were derived from raw *F*-*d* curves by subtracting the cantilever deflection *F*/*k_c* from *d* to obtain δ . In all example studies, the unloading portion of each *F*- δ curve was fit to the Johnson, Kendall, and Roberts (JKR) contact model [28] (the use of which is justified later), which predicts the deformed shape of an elastic half-space in contact with a sphere based on a balance between the elastic and surface energy. At a given *F*, the sphere and flat surface deform a distance δ to form a contact over a circle of radius *a*, given by

$$F = \frac{4E^* a^3}{3R} - 2\sqrt{2\pi E^* w a^3} \quad (1)$$

and

$$\delta = \frac{a^2}{R} - \sqrt{\frac{2\pi a w}{E^*}} \quad (2)$$

where *w* is the work of adhesion and *E** is the reduced modulus of the contact. *E** is a function of the indentation modulus

of the surface M_s and AFM tip M_t , as defined by $1/E^* = 1/M_s + 1/M_t$. From equations (1) and (2), we see that due to adhesive effects the contact area $A = \pi a^2$ is larger than that predicted by the Hertz theory [29], and remains finite until a critical pull-off force is reached, at which point the surfaces separate. In a load-controlled measurement, such as with a compliant AFM cantilever, the magnitude of the critical pull-off force $F_{po} = 3\pi R w / 2$. M_s and F_{po} were extracted from each F - δ data set with a four-step process: (1) assess F_{po} from the retract portion of the F - δ curve as shown in Fig. 1(b), (2) calculate w from F_{po} via $w = 2F_{po} / 3\pi R$, (3) find E^* by fitting the entire F - δ curve to equations (1) and (2) with E^* as the fitting parameter, and (4) calculate M_s from E^* with $M_t = 164.8$ GPa for Si(100) [30]. Additional information on this process can be found elsewhere [31].

Materials

Despite the similarities in the overall experimental methods, the sample preparation for each of the example studies was different; each sample set was prepared in accordance with published protocols for each type of evidence. For the study on trace evidence, Caucasian hair samples were removed from a single source, washed with a commercially-available shampoo for 60 s, rinsed with deionized (DI) water for 60 s, dried in a N_2 gas flow, and stored in aluminum foil under vacuum. Three different types of hair samples were studied: “virgin” hair, “conditioned” hair, and “bleached” hair. The virgin samples were the baseline samples, as no further treatment was applied prior to the AFM measurements. In contrast, the conditioned and bleached hair received additional treatments; the conditioned and bleached hair were exposed to a commercially-available conditioner for 60 s and a commercially-available bleach for 1 h, respectively, and then rinsed with DI water for 60 s, dried in a N_2 flow, and stored in aluminum foil under vacuum [24]. Hair samples (≈ 10 mm long) were mounted onto AFM sample discs via a two-part epoxy only at the sample ends to ensure no interference with the top surface; the adhesion between the hair sample and AFM disc was found to be sufficient to keep the middle of the sample fixed to the disc during AFM measurements.

For the questioned documents study, line crossings were produced on plain copy paper, first with a commercially-available laserjet printer (black ink) and then with a ballpoint pen (blue ink) [9]. The crossed-lines sample (10 mm \times 5 mm) was removed from the paper with a razor blade and mounted onto an AFM sample disc using double-sided tape.

For the study on impression and pattern evidence, fingerprints from a single donor were deposited onto Si (100) surfaces cut to a size of 10 mm \times 10 mm. Prior to fingerprint deposition, the surfaces were cleaned via a multi-step process: rinsed in isopropanol for 5 min, cleaned with 2:1 $H_2SO_4:H_2O_2$ piranha solution for 10 min, rinsed in DI water and

isopropanol for 5 min each, and dried in a N_2 flow. Furthermore, the donor's hands were thoroughly washed and dried to remove any superfluous material. The time allowed for sweat development was ≈ 30 min, after which prints from individual fingers were placed on the clean Si (100) surfaces [19]. The samples were mounted on AFM sample discs via a two-part epoxy and measurements were conducted on portions of the fingerprint over a 3 day period.

For the study on explosive materials, 0.5 % TNT polymer microspheres were fixed to AFM cantilevers via a two-part epoxy. The colloidal probes were brought into contact with 10 mm \times 10 mm sections of cotton and rayon fabrics to assess their affinity for different fabric types. More details on the production and characterization of the polymer microspheres can be found in previous work [32]. In summary, the microspheres were prepared with an oil/water emulsion process using a precision particle fabrication (PPF) nozzle to deliver precisely-controlled microdrops with both the base polymer and explosive material into a water beaker. The PPF operating parameters were varied to regulate the droplet size and the final microsphere diameter. In this study, the base polymer was poly(DL-lactide/glycolide) acid, the explosive analyte was TNT, and the PPF operating parameters were adjusted such that the final microsphere diameter was ≈ 24 μ m.

Results

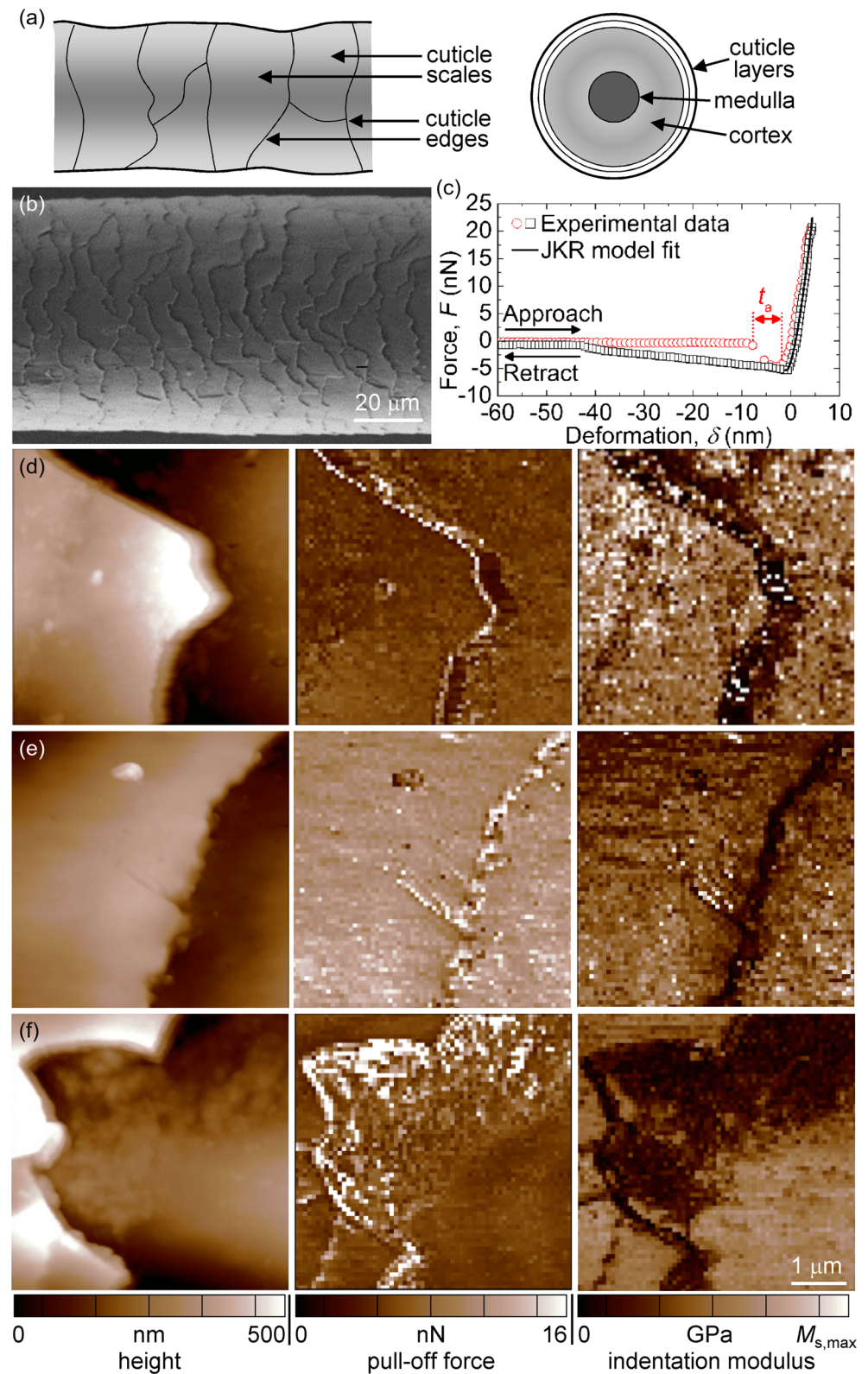
Trace Evidence

Figure 2(a) and (b) show a schematic diagram and SEM image of a hair fiber, respectively. In general, each hair fiber contains three main layers: the cuticle, the cortex, and the medulla. At the surface, the cuticles provide a protective coating via overlapping cells, or scales, with thicknesses of 0.3 μ m to 0.5 μ m and exposed lengths from 5 μ m to 10 μ m. The cuticle layers surround the cortex, which is composed of spindle-shaped cells aligned along the fiber axis and comprises the majority of the hair mass. Finally, thicker hairs often have an additional loosely-packed porous region near the center of the hair, called the medulla. In all, each hair fiber is ≈ 50 μ m to 100 μ m in diameter. A representative F - δ curve on a hair fiber is shown in Fig. 2(c). On approach, the deformation of the sample surface from the initial “snap-in” event to the underlying hair contact point, defined here as t_a , can be related to the thickness of any surface layer (e.g., water, conditioner, contamination) on the hair, whereas during retraction, the F - δ data in the contact region can be fit to the JKR model to extract both the elastic and adhesive properties. Thus, the elastic and adhesive properties of both the hair and its surface layers can be studied by AFM.

AFM height, pull-off force, and indentation modulus data over 5 μ m \times 5 μ m regions for virgin, bleached, and conditioned hair are shown in Fig. 2(d), (e), and (f), respectively. For the



Fig. 2 (a) Schematic diagram and (b) SEM image of a hair fiber. (c) Representative F - δ curve on a hair fiber. On approach, t_a can be used to estimate the surface layer thickness, whereas on retraction, the F - δ data in the contact region can be fit to the JKR model to determine M_s and F_{po} . AFM height (left column), pull-off force (middle column), and indentation modulus (right column) data for (d) virgin, (e) bleached, and (f) conditioned hair. $M_{s,max}$ is 5 GPa for (d) and (e) and 1 GPa for (f)



virgin hair, M_s was determined to be $2.4 \text{ GPa} \pm 1.1 \text{ GPa}$ (unless otherwise noted, the experimental uncertainties throughout this paper are one standard deviation of the sample mean), which is in good agreement with results from instrumented indentation

[33], *in-situ* tensile tests [34], and AFM [24] (2 GPa to 8 GPa). The large uncertainty in the M_s value was due to heterogeneity in the cuticle layers, in particular at the cuticle edges as shown in Fig. 2(d). The bleached hair exhibited a slightly smaller M_s ,

1.8 GPa \pm 0.9 GPa, most likely because the chemical treatment destroyed some of the disulphide cross-links in the cuticles, thereby weakening its mechanical properties [24]. Moreover, F_{po} was found to increase by a factor of two in response to the bleach treatment. Such chemical treatments are known to remove saturated fatty acid lipid layers from the hair surface. As a result, the hair surface becomes more hydrophilic (as shown in contact angle measurements [35]), which increases the thickness of the adsorbed water layer and the pull-off force due to capillary meniscus effects. For the conditioned hair, the average values for M_s and F_{po} were highly dependent on the position along the hair due to heterogeneous conditioner surface coverage, with a majority of the conditioner segregated at the cuticle edges (the latter finding reinforces a surmise from previous work [24]). Overall, the conditioned hair exhibited smaller M_s and larger F_{po} than the virgin hair, consistent with a more compliant and thicker liquid layer on the hair surface. In particular, M_s varied from 0.05 GPa to 0.5 GPa, in good agreement with previous AFM studies [24]. Moreover, it was observed that M_s decreased and F_{po} increased as the conditioner thickness increased, as confirmed by the strong correlations in Fig. 2(f).

From the approach sections of the same F - δ data, average values for t_a were also determined for virgin, bleached, and conditioned hair. It is important to note that t_a is not equal to the surface layer thickness h , and tends to be larger than h by about 2 nm (i.e., $h = t_a - 2$ nm) [24]. Two potential reasons for this offset are: (1) a thin surface layer on the AFM tip [36], and (2) bulging and posterior instability of the liquid film on the hair surface [37]. For the virgin hair, t_a was found to be 4.9 nm \pm 0.5 nm, which translates to an h value of about 3 nm. The bleached hair exhibited a slightly larger t_a , 6.0 nm \pm 0.4 nm, which is consistent with the increase in F_{po} from the surface becoming more hydrophilic and thus adsorbing more water. For the conditioned hair, the average value for t_a was again dependent on the position along the hair; an example of F - δ data for conditioned hair is shown in Fig. 2(c). At the cuticle edges, t_a ranged from \approx 5 nm to \approx 15 nm; areas with larger t_a values corresponded to areas with smaller M_s values and larger F_{po} values, all of which are expected in areas with more conditioner on the hair surface. Away from the cuticle edges, t_a was more uniform, with an average value of 6.6 nm \pm 0.4 nm. The resulting h values for the conditioned hair are consistent with estimates based on material deposition [6]. It is important to note that AFM was utilized here only to identify the *presence* and *thickness* of the surface coating, but with further experiments, could also be used to identify the *composition* of the coating.

Questioned Documents

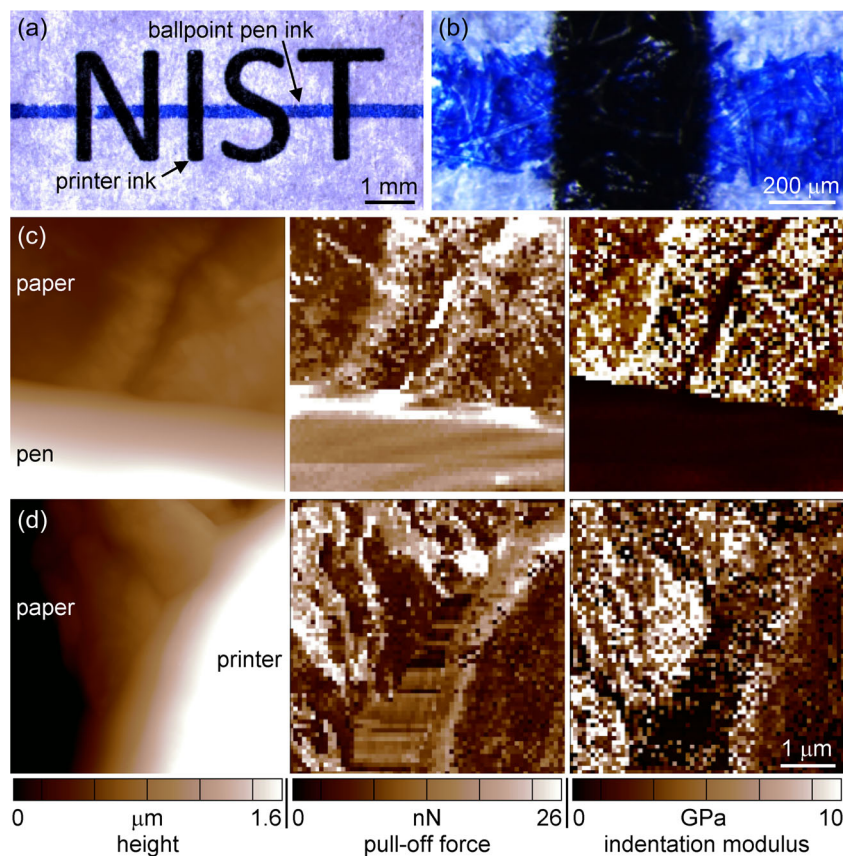
Figure 3(a) and (b) are optical microscope images of multiple line crossings on plain copy paper; in both images, the laserjet printer ink appears black and the ballpoint pen ink appears blue. The printer ink and ballpoint pen ink are similar in that

both appear fairly homogeneous and smooth the surface of the underlying paper, which is rough due to its fibrillar structure. However, higher resolution techniques such as AFM [9], SEM [38–40], and laser profilometry [41] have been used to show that the two inks actually exhibit different morphologies, with the ballpoint ink dense and smooth and the printer ink granular and rough. In addition, these same studies have shown that variations in the surface topography near line crossings can be examined to detect the order in which the inks were placed on the paper. In the following, we show that AFM may provide an additional metric by which to assess the general class of ink and the order in which inks cross, namely the assessment of their mechanical properties.

AFM height, pull-off force, and indentation modulus data over 5 μ m \times 5 μ m regions for pen/paper and printer/paper interfaces are shown in Fig. 3(c) and (d), respectively. In both cases, the height data showed that the ink was deposited on top of the paper, with a step height of \approx 1.2 μ m for both the printer ink and ballpoint pen ink. Conversely, the mechanical properties of the two inks were markedly different; the ballpoint pen ink exhibited M_s and F_{po} of 1.1 GPa \pm 0.2 GPa and 17.3 nN \pm 3.5 nN, respectively, whereas the printer ink showed M_s and F_{po} of 1.8 GPa \pm 0.8 GPa and 6.2 nN \pm 2.5 nN, respectively. These results reveal two important differences between the inks, the first based on the average values for M_s and F_{po} and the second based on the variability in M_s and F_{po} . On the first point, the average values for M_s and F_{po} of the two inks differed by factors of two and three, respectively, with the ballpoint ink exhibiting smaller M_s but greater F_{po} . On the second point, the variability in M_s and F_{po} was also different for the two inks; the ballpoint pen ink exhibited much smaller uncertainties relative to the mean values than the printer ink, which is consistent with previous data that suggest that the ballpoint pen ink is dense and smooth and the printer ink is granular and rough [9, 38–41]. In all, this study provides some of the first quantitative evidence that different inks exhibit different mechanical responses, and thus significantly extends previous qualitative work [9].

Furthermore, the mechanical properties of the underlying paper were considered as shown in Fig. 3(c) and (d). Both M_s and F_{po} were moderately heterogeneous due to the fibrillar structure (i.e., the surface roughness dictates the contact geometry and consequently the measured properties) and composition (i.e., the constituent properties and their proportions dictate the measured properties) of the paper. Despite the variability, the average values for M_s and F_{po} were consistent between the two images, which affords additional support for the differences between the two inks discussed above. In more detail, M_s and F_{po} for the paper were found to be 6.0 GPa \pm 3.6 GPa and 14.2 nN \pm 7.5 nN, respectively. Interestingly, M_s is in good agreement with published values for microcrystalline cellulose (6 GPa to 9 GPa) [42] and at the lower end of the spectrum for nanocrystalline cellulose (6 GPa

Fig. 3 (a) and (b) Optical microscopy images of line crossings on plain copy paper; in both images, the laserjet printer ink is black and the ballpoint pen ink is blue. AFM height (left column), pull-off force (middle column), and indentation modulus (right column) data for (c) pen/paper and (d) printer/paper interfaces



to 50 GPa) [43–45]. The latter disagreement is not surprising given the low crystallinity in the plant and wood fiber used in paper (43 % to 65 %) relative to that in nanocrystalline cellulose (54 % to 100 %) [46].

Impression and Pattern Evidence

Figure 4(a) shows a schematic diagram of a fingerprint impression. As shown, there are two different types of structural characteristics that allow fingerprint examiners to compare impressions and make identifications: *pattern types* and *minutiae*. Pattern types (e.g., arches, loops, and whorls) are class characteristics that are not unique to the individual, while minutiae (e.g., bifurcations, dots, and endings) are features that are unique to the individual [47]. Both pattern types and minutiae are used to match an impression of interest to an impression in a database. However, there are many challenges in the comparison process, mostly due to variability in the (1) residue characteristics, (2) deposition conditions, (3) substrate conditions, (4) environmental conditions, and (5) enhancement methods [48]. For example, the initial residue composition (point 1) is a combination of numerous substances from the epidermis [49], dermis [50], and extrinsic contaminants [51], with the exact properties dependent on the ratio of the three components [48]. Moreover, on point (3), it has been found that the porosity [52] and roughness [18] of the surface

influence the composition and aging kinetics of a fingerprint, as they determine the adsorption rates of the water-soluble compounds in the residue and the effectiveness of the print detection scheme, respectively. As a result of the many confounding factors that contribute to the final characteristics of the print, it is necessary to utilize methods that both “look” and “feel” the print surface, as they not only provide information regarding the print’s owner, but also insight into the print’s composition and age.

Figure 4(b) shows a SEM image of a fingerprint on a silicon surface. The fingerprint ridges were formed by aligned mounds of residue, faintly visible in Fig. 4(b). AFM height data over a $5\ \mu\text{m} \times 5\ \mu\text{m}$ region containing a mound within a single ridge 0 days and 3 days after deposition are shown in Fig. 4(c) and (d), respectively. A cross-section of the data as illustrated in Fig. 4(e) indicates that the maximum height h of the residue decreased from $\approx 200\ \text{nm}$ to $100\ \text{nm}$ over a 3 day period. More importantly, the volume of material decreased during that time, as evident by the decrease in the integrated area under the cross-sectional profiles. The aging process of a fingerprint involves the alteration or disappearance of the initial compounds via degradation, evaporation, migration, and polymerization [48]. The most significant process involves the loss of water via evaporation, as this is the main constituent in fingerprint residue. In detail, one study reported an 85 % reduction in the weight of a fingerprint over a two-week time

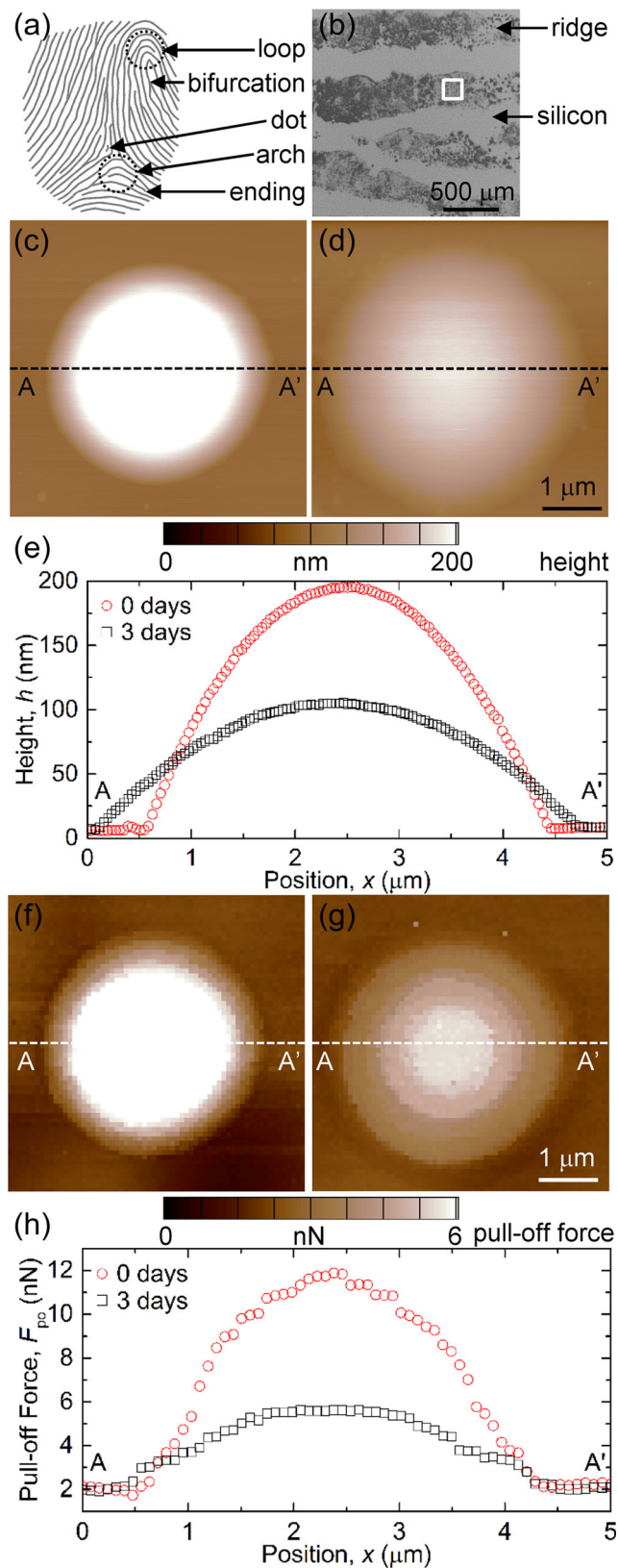


Fig. 4 (a) Schematic diagram of a fingerprint impression, with the pattern types circled for clarity. (b) SEM image of a fingerprint on a silicon surface. AFM height data within a single ridge after (c) 0 days and (d) 3 days; a cross-section of the height data (section AA') is shown in (e). AFM pull-off force data in the same area after (f) 0 days and (g) 3 days; a cross-section of the pull-off force data (section AA') is shown in (h)

suggesting that amino acids are also unstable with time [54]. AFM pull-off force data over the same area after 0 days and 3 days are shown in Fig. 4(f) and (g), respectively. A cross-section of the data as illustrated in Fig. 4(h) also indicates a decrease in F_{po} over a 3 day period. This decrease in F_{po} could simply be attributed to the decrease in the maximum height as shown above, but could also be due to a change in the surface energy of the residue, which would change w and thus F_{po} . This represents some of the first work on the mechanical response of fingerprint residue, and it is clear from the changes in h and F_{po} that AFM is sensitive to changes to both the residue shape and material properties over time.

Explosive Materials

Unlike the three previous example studies, the study on explosive materials was conducted via colloidal-probe AFM, which employs a microscale colloidal sphere as the probe tip. As a result, the probe tip is no longer restricted to silicon or silicon nitride, and can be modified with trace amounts of material (e.g., explosive particles) to conduct adhesion measurements on various surfaces. Such an approach has the potential to augment bulk detection schemes such as X-ray or neutron imaging, which require large quantities of explosive materials, and vapor and particle detection systems such as optical and mass spectroscopy and chromatography, which run into problems with the depressed vapor pressures, small sample sizes, and sampling and surface contaminations commonly associated with many explosives [55]. Accordingly, there have been a number of studies that have used colloidal-probe AFM to examine the adhesion between explosive particles and surfaces, with TNT, RDX, and PETN as the explosives and different model *metals* and *polymers* as the surfaces [22, 23, 25]. In the following, we extend colloidal-probe AFM to assess the adhesion between explosives and different *fabric* types. Explosive/fabric adhesion studies are vital, not only because they provide information regarding a particle's affinity for clothing, but also may enable insight into the efficacy of different detection schemes [56].

Figure 5(a) shows a SEM image of a TNT microsphere attached to an AFM cantilever and Fig. 5(b) and (c) represent optical microscopy images of the cotton and rayon fabrics, respectively. The images of the cotton and rayon fabrics indicate that there are slight differences in the weave, but at higher magnifications, the disparities between the two fabrics became less evident (i.e., individual fibers in the two fabrics

period, which was primarily attributed to water loss [53]. Moreover, the amino acid content in a fingerprint on paper was found to decrease by a factor of two after 236 days,

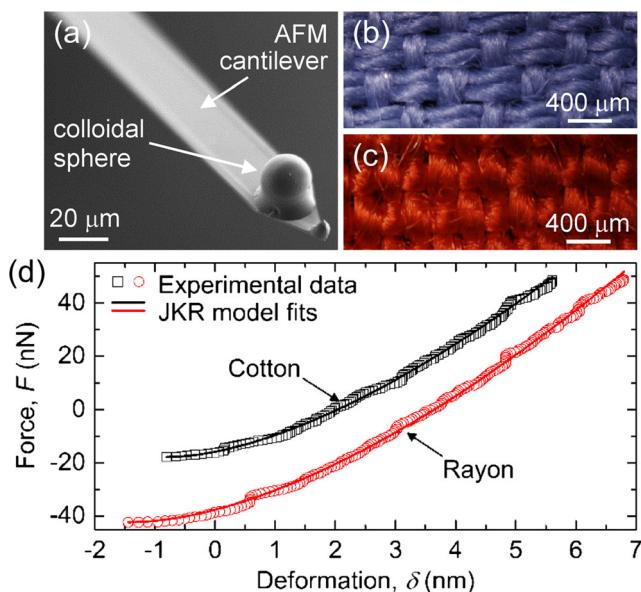


Fig. 5 (a) SEM image of a TNT microsphere probe on an AFM cantilever. Optical microscopy images of the (b) cotton and (c) rayon fabrics. (d) Representative F - δ curves for both the cotton and rayon (retract portions only), along with their respective JKR fits

were found to have diameters of $\approx 20 \mu\text{m}$, in agreement with previous work [57]). Representative F - δ curves for both cotton and rayon (retract portions only) are shown in Fig. 5(d), along with their respective JKR fits. From the fits, it was established that the two fabrics exhibited very similar M_s , i.e., $29.0 \text{ MPa} \pm 8.0 \text{ MPa}$ for the cotton and $30.7 \text{ MPa} \pm 7.0 \text{ MPa}$ for the rayon. Two potential reasons that the M_s values are considerably smaller than those reported [57] for individual cotton and rayon fibers (3 GPa to 11 GPa) include: (1) the microsphere is in contact with multiple fibers and/or (2) the fibers in the fabric are loosely bound thus allowing them to bend in response to the applied force. In contrast, the two fabrics exhibited markedly different F_{po} ; in more detail, the pull-off force between TNT and rayon was a factor of two greater than that between TNT and cotton. Two potential explanations for the change in F_{po} include differences in the surface roughness and work of adhesion. On the first point, one study showed that certain combinations of roughness between the particle and surface brought about preferred particle-surface orientations, thus producing larger values for F_{po} (i.e., larger contact areas give rise to larger pull-off forces) [23]. On the second point, another study discovered that certain surface chemistries brought about larger w , again resulting in larger values for F_{po} (i.e., $-\text{OH}$ and $-\text{C}_6\text{H}_5$ end groups give rise to larger pull-off forces) [25].

Discussion and Conclusions

The example studies presented here demonstrate that AFM can be used for both topographic imaging and quantitative

mechanical properties measurements of materials that often appear as forensic evidence, in this case hair, ink, fingerprint residue, and explosive particles. A very simple measurement procedure of an approach-retract sequence for the AFM cantilever followed by subtraction of the cantilever displacement from the raw force-displacement output led to the force-deformation data characterizing the probe-sample interaction. Analysis of these data using a well-established model [28] enabled quantitative determination of the adhesion between the probe and sample and the stiffness of the sample. The use of this particular model is justified here, given that the Tabor parameter [58] μ varied from 4 to 8 for the first three case studies and was ≈ 500 for the last study, based on R values from SEM, M_s and w values from AFM, and an equilibrium separation of $z_0 = 0.2 \text{ nm}$ from ref. [59]. However, for other forms of evidence, R , M_s , w , and z_0 will change and different contact models may be more appropriate [60]. Furthermore, the pull-off forces and moduli obtained were able to clearly distinguish various treatments of hair, types of ink, age of fingerprints, and composition of fabrics, and related these to structure of the sample (e.g., broken bonds in the hair, granularity of the ink). Mapping of the properties provided a sense of the homogeneity of the materials and enabled statistically significant numbers of measurements to be performed. As an example, the M_s and F_{po} measurements in the first three case studies were carried out at each node of a 64×64 grid over a $5 \mu\text{m} \times 5 \mu\text{m}$ area, leading to means and standard deviations based on >4000 data points.

The last point above is particularly important with regard to needs in forensic research defined in a recent National Academy of Sciences report [61]: studies establishing the scientific bases demonstrating the validity of forensic methods and development of quantifiable measures of the reliability, accuracy, and uncertainty of forensic analyses. The research also addresses needs in forensic science identified by the National Institute of Justice [62]: improved capability to expand the information extracted from evidence and to quantify its evidentiary value. The measurements here of mechanical properties generated well-defined means and standard deviations for the measured quantities and are thus examples of the first step in establishing AFM as a useful forensic evidence tool. These quantities enable the second step of straightforward tests and quantitative specification of the statistical significance of the perceived similarities or differences in properties. Such specification relies on the precision of the measurements (that is, how tightly the measured quantities group about the mean value). In order to ensure adequate precision for useful AFM forensic studies, methods will need to be developed to examine statistically relevant sample numbers and to search large areas for small items. Comparison of properties measured in different laboratories or with standard samples will require specification of the accuracy of the measurements (that is, how closely the measured mean value

approaches a “true” or accepted value). Accuracy of AFM for forensic studies will require calibrations methods for the displacements of the xy scanner and the z piezo (as these determine the length scales of the measurements) and the stiffness of the cantilever (as this determines both the force sensitivity and the relation between z piezo displacement and probe-sample deformation). Specification of accuracy will require standard artifacts for use as reference materials that can be measured in different laboratories. Such artifacts might include standard hair, fibers, and particles. In addition, collected pieces of evidence will inevitably contain surface dust, dirt, or liquid films, and the potentially confounding effects of such surface residue on both the precision and accuracy of AFM measurements will need to be quantified. Finally, it is to be recognized that as with all techniques, building of an experience base for quantitative AFM forensic evidence generation is required in order to build trust in AFM techniques. Pervasive availability of appropriate instruments, training, protocols, and standards is thus required.

References

- O'Connor SD, Komisarek KL, Baldeschwieler JD (1995) Atomic force microscopy of human hair cuticles: a microscopic study of environmental effects on hair morphology. *J Invest Dermatol* 105:96–99
- You H, Yu L (1997) Atomic force microscopy as a tool for study of human hair. *Scanning* 19:431–437
- McMullen RL, Kelty SP (2001) Investigation of human hair fibers using lateral force microscopy. *Scanning* 23:337–345
- Blach J, Loughlin W, Watson G, Myhra S (2001) Surface characterization of human hair by atomic force microscopy in the imaging and F-d modes. *Int J Cosmet Sci* 23:165–174
- Gurden SP, Monteiro VF, Longo E, Ferreira MMC (2004) Quantitative analysis and classification of AFM images of human hair. *J Microscopy* 215:13–23
- LaTorre C, Bhushan B (2005) Nanotribological characterization of human hair and skin using atomic force microscopy. *Ultramicroscopy* 105:155–175
- Bhushan B, Chen N (2006) AFM studies of environmental effects on nanomechanical properties and cellular structure of human hair. *Ultramicroscopy* 106:755–764
- Chen Y-F (2011) Forensic applications of nanotechnology. *J Chin Chem Soc* 58:828–835
- Kasas S, Khanmy-Vital A, Dietler G (2001) Examination of line crossings by atomic force microscopy. *Forensic Sci Int* 119:290–298
- D'Uffizi M, Falso G, Ingo GM, Padeletti G (2002) Microchemical and micromorphological features of gunshot residue observed by combined use of AFM, SA-XPS, and SEM + EDS. *Surf Interf Anal* 34:502–506
- Mou Y, Lakadwar J, Rabalais JW (2008) Evaluation of shooting distance by AFM and FTIR/ATR analysis of GSR. *J Forensic Sci* 53:1381–1386
- Sharma J, Teter JP, Abbundi RJ, Guardala NA (2003) Determination of radiation exposure history of common materials and computer hardware by using atomic (and magnetic force) microscopy. *Appl Phys Lett* 82:2236–2238
- Chen Y, Cai J (2006) Membrane deformation of unfixed erythrocytes in air with time lapse investigated by tapping mode atomic force microscopy. *Micron* 37:339–346
- Strasser S, Zink A, Kada G, Hinterdorfer P, Peschel O, Heckl WM, Nerlich AG, Thalhammer S (2007) Age determination of blood spots in forensic medicine by force spectroscopy. *Forensic Sci Int* 170:8–14
- Wu Y, Hu Y, Cai J, Ma S, Wang X, Chen Y, Pan Y (2009) Time-dependent surface adhesive force and morphology of RBC measured by AFM. *Micron* 40:359–364
- Science and Technology Review, https://www.llnl.gov/str/Sep06/pdfs/09_06.2.pdf
- Watson GS, Watson JA (2007) Potential applications of scanning probe microscopy in forensic science. *J Phys Conference Series* 61:1251–1255
- Jones BJ, Downham R, Sears VG (2010) Effect of substrate surface topography on forensic development of latent fingerprints with iron oxide powder suspension. *Surf Interf Anal* 42:438–442
- Goddard AJ, Hillman AR, Bond JW (2010) High resolution imaging of latent fingerprints by localized corrosion on brass surfaces. *J Forensic Sci* 55:58–65
- Canetta E, Montiel K, Adya AK (2009) Morphological changes in textile fibers exposed to environmental stresses: atomic force microscopic examination. *Forensic Sci Int* 191:6–14
- Canetta E, Adya AK (2011) Atomic force microscopic investigation of commercial pressure sensitive adhesives for forensic analysis. *Forensic Sci Int* 210:16–25
- Taylor DE, Strawhecker KE, Shanholtz ER, Sorescu DC, Sausa RC (2014) Investigations of the intermolecular forces between RDX and polyethylene by force–distance spectroscopy and molecular dynamics simulations. *J Phys Chem A* 118:5083–5097
- Chaffee-Cipich MN, Sturtevant BD, Beaudoin SP (2013) Adhesion of explosives. *Anal Chem* 85:5358–5366
- Chen N, Bhushan B (2006) Atomic force microscopy studies of conditioner thickness distribution and binding interactions on the hair surface. *J Microscopy* 221:203–215
- Zakon Y, Lemcoff NG, Marmur A, Zeiri Y (2012) Adhesion of standard explosive particles to model surfaces. *J Phys Chem C* 116:22815–22822
- Cook RF (2010) Mechanics of adhesion. In: Oyen ML (ed) *Handbook of nanoindentation with biological applications*. Pan Stanford Publishing, Singapore, pp 77–121
- Hutter JL, Bechhoefer J (1993) Calibration of atomic-force microscope tips. *Rev Sci Instrum* 64:1868–1873
- Johnson KL, Kendall K, Roberts AD (1971) Surface energy and the contact of elastic solids. *Proc Roy Soc A* 324:301–313
- Hertz H (1881) On the contact of elastic solids. *J Reine Angew Math* 92:156–171
- Vlassak JJ, Nix WD (1993) Indentation modulus of elastically anisotropic half spaces. *Phil Mag A* 67:1045–1056
- DelRio FW, Steffens KL, Jaye C, Fischer DA, Cook RF (2009) Elastic, adhesive, and charge transport properties of a metal–molecule–metal junction: the role of molecular orientation, order, and coverage. *Langmuir* 26:1688–1699
- Staymates M, Fletcher R, Staymates J, Gillen G, Berkland C (2010) Production and characterization of polymer microspheres containing trace explosives using precision particle fabrication technology. *J Microencapsulation* 27:426–435
- Wei G, Bhushan B, Torgerson PM (2005) Nanomechanical characterization of human hair using nanoindentation and SEM. *Ultramicroscopy* 105:248–266
- Seshadri IP, Bhushan B (2008) *In situ* deformation characterization of human hair with atomic force microscopy. *Acta Mater* 56:774–781



35. Lodge RA, Bhushan B (2006) Wetting properties of human hair by means of dynamic contact angle measurements. *J Appl Polym Sci* 102:5255–5265
36. Bhushan B, Blackman GS (1991) Atomic force microscopy of magnetic rigid disks and sliders and its applications to tribology. *J Tribol Trans ASME* 113:452–457
37. Forcada ML, Jakas MM, Grasmarti A (1991) On liquid film thickness measurements with the atomic force microscope. *J Chem Phys* 95:706–708
38. Waeschle PA (1979) Examination of line crossings by scanning electron microscopy. *J Forensic Sci* 24:569–578
39. Koons RD (1985) Sequencing of intersecting lines by combined lifting process and scanning electron microscopy. *Forensic Sci Int* 27:261–276
40. Blueschke A, Lacin A (1996) Examination of line crossings by low KV scanning electron microscopy (SEM) using photographic stereoscopic pairs. *J Forensic Sci* 41:80–85
41. Spagnolo GS (2006) Potentiality of 3D laser profilometry to determine the sequence of homogeneous crossing lines on questioned documents. *Forensic Sci Int* 164:102–109
42. Das K, Ray D, Bandyopadhyay NR, Ghosh T, Mohanty AK, Misra M (2009) A study of the mechanical, thermal, and morphological properties of microcrystalline cellulose particles prepared from cotton slivers using different acid concentrations. *Cellulose* 16:783–793
43. Lahiji RR, Xu X, Reifengerger R, Raman A, Rudie A, Moon RJ (2010) Atomic force microscopy characterization of cellulose nanocrystals. *Langmuir* 26:4480–4488
44. Postek MT, Vladar A, Dagata J, Farkas N, Ming B, Wagner R, Raman A, Moon RJ, Sabo R, Wegner TH, Beecher J (2011) Development of the metrology and imaging of cellulose nanocrystals. *Meas Sci Technol* 22:024005
45. Wagner R, Moon R, Pratt J, Shaw G, Raman A (2011) Uncertainty quantification in nanomechanical measurements using the atomic force microscope. *Nanotechnology* 22:455703
46. Moon RJ, Martini A, Nairn J, Simonsen J, Youngblood J (2011) Cellulose nanomaterials review: structure, properties, and nanocomposites. *Chem Soc Rev* 40:3941–3994
47. Daluz HM (2015) *Fundamentals of fingerprint analysis*. CRC Press, Boca Raton
48. Girod A, Ramotowski R, Weyermann C (2012) Composition of fingermark residue: a qualitative and quantitative review. *Forensic Sci Int* 223:10–24
49. Drapel V, Becue A, Champod C, Margot P (2009) Identification of promising antigenic component in latent fingermark residue. *Forensic Sci Int* 184:47–53
50. Reinholz AD (2008) Albumin development method to visualize friction ridge detail on porous surface. *J Forensic Ident* 58:524–539
51. Croxton RS, Baron MG, Butler D, Kent T, Sears VG (2010) Variation in amino acids and lipid composition of latent fingerprints. *Forensic Sci Int* 199:93–102
52. Weyermann C, Roux C, Champod C (2011) Initial results on the composition of fingerprints and its evolution as a function of time by GC/MS analysis. *J Forensic Sci* 56:102–108
53. Mong GM, Petersen CE, Clauss TRW (1999) Advanced fingerprint analysis project fingerprint constituents. Pacific Northwest National Laboratory, Report# PNNL-13019
54. Cuthbertson F (1969) The chemistry of fingerprints. United Kingdom Atomic Energy Authority, Report# AWRE 013/69
55. Steinfeldt JI, Wormhoudt J (1998) Explosives detection: a challenge for physical chemistry. *Annu Rev Phys Chem* 49:203–232
56. Verkouteren JR, Coleman JL, Fletcher RA, Smith WJ, Klouda GA, Gillen G (2008) A method to determine collection efficiency of particles by swipe sampling. *Meas Sci Technol* 19:115101
57. Bunsell AR (2009) Introduction to fibre tensile properties and failure. In: Bunsell AR (ed) *Handbook of tensile properties of textile and technical fibres*. Woodhead Publishing, Cambridge, pp 1–17
58. Tabor D (1977) Surface forces and surface interactions. *J Colloid Interface Sci* 58:2–13
59. Israelachvili J (1991) *Intermolecular and surface forces*, 2nd edn. Academic, London
60. Maugis D (1992) Adhesion of spheres: the JKR-DMT transition using a Dugdale model. *J Colloid Interface Sci* 150:243–269
61. Strengthening forensic science in the United States: A path forward: National Research Council (2009)
62. National Institute of Justice, Forensic Sciences, <http://nij.gov/topics/forensics/welcome.htm>

